2024 European Control Conference (ECC)
June 25-28, 2024. Stockholm, Sweden

Design and Control of a VTOL Aerial Vehicle Tilting its Rotors Only with Rotor Thrusts and a Passive Joint

Takumi Ito[1], Riku Funada[1], and Mitsuji Sampei[1]

Abstract— **This paper presents a novel VTOL UAV that owns a link connecting four rotors and a fuselage by a passive joint, allowing the control of the rotor's tilting angle by adjusting only the rotors' thrust. This unique structure contributes to eliminating additional actuators, such as servo motors, to control the tilting angles of rotors, resulting in the UAV's weight lighter and simpler structure. We first derive the dynamical model of the newly designed UAV and analyze its controllability. Then, we design the controller that leverages the tiltable link with four rotors to accelerate the UAV while suppressing a deviation of the UAV's angle of attack from the desired value to restrain the change of the aerodynamic force. Finally, the validity of the proposed control strategy is evaluated in simulation study.**

I. INTRODUCTION

Unmanned aerial vehicles (UAVs) have been employed in many application fields, including agriculture [1], transportation [2], and search and rescue [3]. In these application domains, various types of UAVs are utilized, and most of the traditional ones can be categorized into fixed-wing or multi-rotor UAVs. Both of them have their own advantages. For example, a fixed-wing UAV tends to have a superior cruising distance, and a multi-rotor UAV can achieve static hovering, as discussed in [4]. Hence, choosing an appropriate category of UAV for a task is a crucial factor for mission performance. Still, several applications require favorable properties of both fixed-wing and multi-rotor UAVs, e.g., transportation tasks tend to favor UAVs with long cruising distance, which only requires a small takeoff and landing area.

One of the prospective approaches to integrating beneficial features of both fixed-wing and multi-rotor UAVs is to design a hybrid UAV, which has a wing and is capable of vertical takeoff and landing (VTOL) [5]. Generally, hybrid UAVs are classified into two classes: one is a tail-sitter, and the other is a convertible UAV. A tail-sitter takes off and lands vertically on its tail, while a convertible UAV keeps its fuselage in a horizontal direction in all the cruising, landing, and takeoff phases. While many tail-sitter UAVs have shown successful results [6], [7], [8], convertible UAVs are more prevailing than the tail-sitter so far, partially due to the simple mechanism, smooth transitions, and more robust stability in the hovering phase, as mentioned in [5].

Because of the variety of convertible UAVs' structure designs and challenges in control, various control methodologies are proposed to achieve cruising, VTOL, and phase transitions. In [9], a control strategy of transition from cruising to hovering flight is designed based on maneuverability analysis for a dual propulsion UAV, which has both upward and horizontally directed rotors for generating thrust for hovering and cruise flight. Other than dual convertible UAVs, several studies have presented control methods for convertible UAVs having tiltable rotors or a wing [10]. The work [11] has proposed a controller for a convertible UAV with two tiltable rotors based on the gain scheduling technique. They have also presented another control strategy based on the total energy control system design [12]. Nonlinear control techniques are also applied to convertible UAVs, e.g., nonlinear dynamic inversion [13] and nonlinear model predictive control [14], [15]. The fault tolerant control for an actuator failure is also considered in [16]. All the above papers, which consider a convertible UAV with tiltable rotors or wings, necessitate additional actuators, such as servo motors, for controlling the tilting angle of rotors or wings. Although this additional mechanism makes it easy to control these tilting angles, it leads to an increase in the weight and could make the maintenance cumbersome. Chiappinelli et al. integrated a passive rotary joint into the tilting mechanism, which decouples the tilting control [17]. However, this UAV still requires control surfaces like an aileron or elevator, increasing weight and complicating control.

This paper presents a novel convertible UAV with tiltable rotors, which control its rotors' tilting angles only by rotor thrusts and a passive joint without additional actuators, including control surfaces. More concretely, the proposed UAV owns four rotors mounted on a link, which is connected to the fuselage by a passive joint, and two fixed rotors at the tail, as shown in Fig. 1. This unique structure enables us to control the tilting angles of four rotors in front by adjusting their rotor thrusts. Therefore, the design reduces the weight of the tilting mechanism. We first derive the equation of motion of this UAV and analyze its controllability. The derived condition for controllability is then utilized to plan the angle of attack of the body and the tilting angle of the link having four rotors. Second, we propose a controller that utilizes a tiltable link with four rotors to control the UAV's speed while the UAV's angle of attack follows the value planned from the equilibrium conditions. Finally, the effectiveness of the proposed control method is demonstrated via simulation study.

A. Notation

A scaler variable is denoted by lower-case or upper-case symbols as a or A. A vector is denoted by a bold lower-

*This work was supported by JSPS KAKENHI, Grant Number 21H01348 and JST SPRING Grant Number JPMJSP2106.

[1] Department of Systems and Control Engineering, Tokyo Institute of Technology, takumi.ito@sl.sc.e.titech.ac.jp. {funada},{sampei}@sc.e.titech.ac.jp.

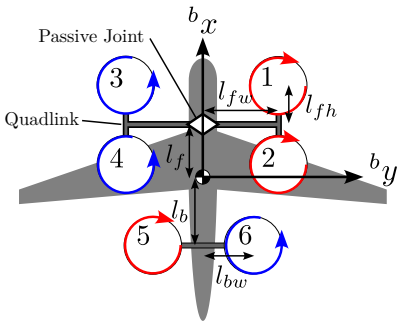

Fig. 1: Topview of the proposed UAV.

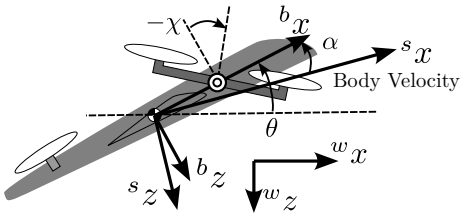

Fig. 2: Sideview of the proposed UAV.

case as $\boldsymbol{a}$, while a matrix is denoted by a bold upper-case as $\boldsymbol{A}$. The $n \times m$ zero matrix is denoted as $\boldsymbol{O}_{n\times m}$. The $n \times n$ zero matrix and identity matrix are denoted as $\boldsymbol{O}_n$ and $\boldsymbol{I}_n$, respectively. The zero vector is denoted as $\mathbf{0}$, whose size is obvious in each situation. The rotational matrix corresponding to the x-axis is denoted as $\boldsymbol{R}_x$, similarly for the y- and z-axes. $\cos(*)$ and $\sin(*)$ will be sometimes denoted as C_* and S_* for notational simplicity.

II. MODELING

This section presents a novel design of a VTOL aerial vehicle shown in Fig. 1. We first describe the overall picture of the proposed UAV while introducing several flight modes that will be considered in the paper. We then clarify that the dynamical equation of the UAV is composed of two factors: the rotor thrusts and the aerodynamics of the wing. The forces and torques rendered by these two factors are calculated in the later part of this section.

A. Overview of the Vehicle

Let us first introduce several coordinate frames, which are illustrated in Fig. 2. The inertial frame Σ_w is fixed to the ground aligned with the North-East-Down (NED) direction. The body-fixed frame Σ_b is arranged at the center of mass of the vehicle so that its x-axis, y-axis, and z-axis are directed forward, right, and downward of the fuselage. In addition to these two frames, we introduce the stability frame Σ_s, which is obtained by rotating the body frame Σ_b around the y-axis to make the velocity in the z-axis of Σ_s zero. Note that this rotational angle around the y-axis from Σ_s to Σ_b is referred to as the angle of attack, denoted as α hereafter. The link frame Σ_ℓ is fixed to the center of the quadlink, and its rotation angle around the y-axis to the body frame is denoted as χ hereafter. Each rotor also has its own coordinate frame, where its origin is located at the center

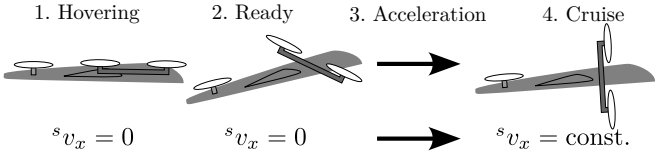

Fig. 3: Flight modes considered in this paper.

of the rotor. The attitude of the first to fourth rotor frames aligns with the quadlink frame and the fifth and sixth with the body frame. A left-side superscript of the variables signifies coordinate frame, where b, w, s, ℓ, and r_i mean the body, inertial, stability, link, and the ith rotor's frame, respectively.

The overview of the proposed VTOL UAV is depicted in Figs. 1 and 2. The UAV comprises a fuselage, six rotors, and a link connecting four rotors and a fuselage by a passive joint. The link can freely rotate around the y-axis of Σ_ℓ and is referred to as the quadlink since it owns the first to fourth rotors. The remaining two rotors, fifth and sixth, are fixed to the tail of the body. The size of the quadlink and the rotors' configurations are defined with l_f, l_{fw}, l_{fh}, l_b, and l_{bw}, as shown in Fig. 1. Note that there are two types of rotors: a positive (P) rotor and a negative (N) rotor, depicted as red and blue in Fig. 1. The P rotor rotates clockwise, and the N rotor counterclockwise. The value of χ reaches 0 when the rotors are directed upward of the body and reaches $-\pi/2$ when they are oriented fully forward of the body. The control of χ is achieved by manipulating the thrust of the rotors within the quadlink.

The proposed UAV distinguishes itself from conventional tiltrotor VTOL UAVs because of its unique tilting mechanism of rotors, which relies on a passive joint controlled solely by rotor thrusts. It is noteworthy that the presented UAV is controlled without any control surfaces, such as a rudder, aileron, or elevator. This design strategy allows us to eliminate additional actuators other than rotors, resulting in a reduction in overall weight and simplicity of structure.

One of the most challenging aspects of VTOL UAV control lies in the transition from hovering mode to cruise flight mode. To address this challenge, we employ a four-phase transition strategy as shown in Fig. 3. The four transition phases are as follows:

1) Hovering Phase: During this phase, the vehicle takes off vertically and remains in a static hover in mid-air. The thrust of four rotors connected to quadlink is controlled to maintain $\chi = 0$ during this phase.
2) Ready Phase: The vehicle smoothly transitions to the planned initial α and χ suitable for starting the acceleration phase while the position of the UAV still keeps the same value as the hovering phase.
3) Acceleration Phase: The vehicle accelerates forward during this phase until it reaches the desired forward velocity. For this goal, we design a control framework that tilts the quadlink forward to increase the UAV's speed while retaining the angle of attack to the desired value. We achieve this strategy by applying exact linearization, which eliminates the interference between

the angle of attack and other state variables.

4) Cruise Phase: The vehicle maintains stable flight while keeping the forward velocity constant value.

The controller realizing these phases and transitions will be presented in Section IV.

B. Equation of Motion

The position of the vehicle in the inertial frame is denoted as ${}^w\boldsymbol{x} \in \mathbb{R}^3$. The orientation of the body frame in the inertial frame is defined as Y-X-Z Euler angle and represented with the rotation matrix $\boldsymbol{R}(\boldsymbol{\eta}) = \boldsymbol{R}_z(\psi)\boldsymbol{R}_x(\phi)\boldsymbol{R}_y(\theta)$ with the vector $\boldsymbol{\eta} = [\phi\ \theta\ \psi]^\top \in \mathbb{R}^3$. Let us also introduce the body velocity ${}^b\boldsymbol{v} \in \mathbb{R}^3$ and body angular velocity ${}^b\boldsymbol{\omega} \in \mathbb{R}^3$: the linear and angular velocity of the origin of the body frame relative to the inertial frame, as viewed in the current body fixed frame.

As previously mentioned, the proposed vehicle has both rotors and a wing, and each of them generates the force and torque, whose point of application can be modeled to be the vehicle's center of mass. Let us denote the force and torque generated by all the rotors in Σ_b as ${}^b\boldsymbol{f}_{\text{rot}} \in \mathbb{R}^3$ and ${}^b\boldsymbol{\tau}_{\text{rot}} \in \mathbb{R}^3$, which can be calculated by coordinate transformation and the summation of all rotors' thrusts, as detailed later. Also, we introduce the force and torque generated by the aerodynamic force of a wing in Σ_s as ${}^s\boldsymbol{f}_{\text{aero}} \in \mathbb{R}^3$ and ${}^s\boldsymbol{\tau}_{\text{aero}} \in \mathbb{R}^3$, respectively. Then, the total thrust and moment around the center of mass of the vehicle can be expressed as

$$ {}^b\boldsymbol{f} = {}^b\boldsymbol{f}_{\text{rot}} + \boldsymbol{R}_y(\alpha)^\top {}^s\boldsymbol{f}_{\text{aero}} + \boldsymbol{R}(\boldsymbol{\eta})^\top m\boldsymbol{g}, \tag{1} $$

$$ {}^b\boldsymbol{\tau} = {}^b\boldsymbol{\tau}_{\text{rot}} + \boldsymbol{R}_y(\alpha)^\top {}^s\boldsymbol{\tau}_{\text{aero}}, \tag{2} $$

where $\boldsymbol{g} = [0\ 0\ g]^\top$ is the gravitational acceleration.

The mass and the inertial tensor of the vehicle are denoted as $m \in \mathbb{R}$ and $\boldsymbol{J} \in \mathbb{R}^{3\times3}$, respectively. Then, the equation of motion for the vehicle can be expressed as

$$ {}^w\dot{\boldsymbol{x}} = \boldsymbol{R}(\boldsymbol{\eta}){}^b\boldsymbol{v}, \tag{3a} $$

$$ \dot{\boldsymbol{\eta}} = \begin{bmatrix} \cos(\theta) & 0 & \sin(\theta) \\ \sin(\theta)\tan(\phi) & 1 & -\cos(\theta)\tan(\phi) \\ -\sin(\theta)/\cos(\phi) & 0 & \cos(\theta)/\cos(\phi) \end{bmatrix} {}^b\boldsymbol{\omega}, \tag{3b} $$

$$ m{}^b\dot{\boldsymbol{v}} = -{}^b\boldsymbol{\omega} \times (m{}^b\boldsymbol{v}) + {}^b\boldsymbol{f}, \tag{3c} $$

$$ \boldsymbol{J}{}^b\dot{\boldsymbol{\omega}} = -{}^b\boldsymbol{\omega} \times \boldsymbol{J}{}^b\boldsymbol{\omega} + {}^b\boldsymbol{\tau}. \tag{3d} $$

In the following subsections, we derive ${}^b\boldsymbol{f}_{\text{rot}}$, ${}^b\boldsymbol{\tau}_{\text{rot}}$, ${}^s\boldsymbol{f}_{\text{aero}}$, and ${}^s\boldsymbol{\tau}_{\text{aero}}$ in Eqs. (1) and (2).

C. Transformation of the Rotor Thrusts

Each rotor generates the thrust force f_i to the direction of the rotation axis while simultaneously rendering the counter torque τ_i to the opposite direction of the rotation. As in [18], we suppose that the proportional relationship holds between τ_i and f_i as $\tau_i = \kappa_i f_i$, where κ_i is named as the counter torque constant with $\kappa_i = \kappa$ for the P rotor and $\kappa_i = -\kappa$ for the N rotor. Let us define the wrench of ith rotor, which combines the thrust force and torque generated by ith rotor, seen in Σ_{r_i}, as

$$ {}^{r_i}\boldsymbol{f}_i = \begin{bmatrix} 0 & 0 & f_i & 0 & 0 & \kappa_i f_i \end{bmatrix}^\top. \tag{4} $$

The force and torque generated by all rotors constituting the quadlink can be calculated by transforming the above wrench to the quadlink frame Σ_ℓ by employing the adjoint transformation [19] and summing up all four rotors as

$$ \begin{bmatrix} {}^\ell\boldsymbol{f}_{\text{rot}} \\ {}^\ell\boldsymbol{\tau}_{\text{rot}} \end{bmatrix} = \sum_{i=1}^{4} \begin{bmatrix} \boldsymbol{I}_3 & \boldsymbol{O}_3 \\ \hat{\boldsymbol{p}}_{\ell r_i} & \boldsymbol{I}_3 \end{bmatrix} {}^{r_i}\boldsymbol{f}_i, \tag{5} $$

where $\boldsymbol{p}_{\ell r_i}$ represents the relative position of Σ_{r_i} with respect to Σ_ℓ, and hereafter, the vector $\boldsymbol{p}_{**}$ means the same way. Note that the operator $\hat{*} : \mathbb{R}^3 \to so(3) := \{\boldsymbol{S} \in \mathbb{R}^{3\times3} \mid \boldsymbol{S} + \boldsymbol{S}^\top = \boldsymbol{O}_3\}$ provides $\hat{\boldsymbol{a}}\boldsymbol{b} = \boldsymbol{a} \times \boldsymbol{b}$ for any 3D vectors.

The quadlink is connected to the fuselage via a passive joint. Assuming the friction of this passive joint can be negligible, the torque around the y-axis of the quadlink is utilized only for the control of tilting angles of the quadlink. With this setting, the torque rotating the quadlink can be expressed as

$$ \tau_\chi = {}^\ell\tau_{\text{rot}y}. \tag{6} $$

The forces and the remaining torques are transmitted to the fuselage, which can be expressed in the body frame as

$$ \begin{bmatrix} {}^b\boldsymbol{f}_{\text{rot}} \\ {}^b\boldsymbol{\tau}_{\text{rot}} \end{bmatrix} = \begin{bmatrix} \boldsymbol{R}_y(\chi) & \boldsymbol{O}_3 \\ \hat{\boldsymbol{p}}_{b\ell}\boldsymbol{R}_y(\chi) & \boldsymbol{R}_y(\chi) \end{bmatrix} \begin{bmatrix} {}^\ell\boldsymbol{f}_{\text{rot}} \\ {}^\ell\tau_{\text{rot}x} \\ 0 \\ {}^\ell\tau_{\text{rot}z} \end{bmatrix} + \sum_{i=5}^{6} \begin{bmatrix} \boldsymbol{I}_3 & \boldsymbol{O}_3 \\ \hat{\boldsymbol{p}}_{br_i} & \boldsymbol{I}_3 \end{bmatrix} {}^{r_i}\boldsymbol{f}_i. \tag{7} $$

Let us define the rotor thrust vector as $\boldsymbol{f}_{\text{rot}} = [f_1 \cdots f_6]^\top$. Then, Eqs. (6) and (7) can be expressed in a matrix form as

$$ \begin{bmatrix} {}^b\boldsymbol{f}_{\text{rot}} \\ {}^b\boldsymbol{\tau}_{\text{rot}} \end{bmatrix} = \begin{bmatrix} \boldsymbol{\lambda}_1 & \boldsymbol{\lambda}_1 & \boldsymbol{\lambda}_2 & \boldsymbol{\lambda}_2 & \boldsymbol{\lambda}_3 & \boldsymbol{\lambda}_4 \end{bmatrix} \boldsymbol{f}_{\text{rot}}, \tag{8} $$

$$ \tau_\chi = \begin{bmatrix} l_{fh} & -l_{fh} & l_{fh} & -l_{fh} \end{bmatrix} \boldsymbol{f}_{\text{rot}}, \tag{9} $$

where

$$ \boldsymbol{\lambda}_1 = \begin{bmatrix} -S_\chi & 0 & -C_\chi & -l_{fw}C_\chi - \kappa S_\chi & l_f C_\chi & l_{fw}S_\chi - \kappa C_\chi \end{bmatrix}^\top, $$

$$ \boldsymbol{\lambda}_2 = \begin{bmatrix} -S_\chi & 0 & -C_\chi & l_{fw}C_\chi + \kappa S_\chi & l_f C_\chi & -l_{fw}S_\chi + \kappa C_\chi \end{bmatrix}^\top, $$

$$ \boldsymbol{\lambda}_3 = \begin{bmatrix} 0 & 0 & -1 & -l_{bw} & -l_b & \kappa \end{bmatrix}^\top, $$

$$ \boldsymbol{\lambda}_4 = \begin{bmatrix} 0 & 0 & -1 & l_{bw} & -l_b & -\kappa \end{bmatrix}^\top. $$

Notice that the first and second columns in (8) are the same. Similarly, the third and fourth columns in (8) are equal. This signifies that the wrench of two rotors on the same side of the quadlink is equivalent. This fact motivates us to regard the two rotors on the same side as one P or N rotor by introducing the rotor input vector $\boldsymbol{f}_{\text{r+}} = [f_1 + f_2\ f_3 + f_4\ f_5\ f_6]^\top$. Then, the UAV can be modeled like a quadrotor UAV with two tiltable rotors in front as

$$ \begin{bmatrix} {}^b f_{\text{rot}x} \\ 0 \\ {}^b f_{\text{rot}z} \\ {}^b\boldsymbol{\tau}_{\text{rot}} \end{bmatrix} = \boldsymbol{M}(\chi)\boldsymbol{f}_{\text{r+}}, \tag{10} $$

$$ \boldsymbol{M}(\chi) = \begin{bmatrix} \boldsymbol{\lambda}_1 & \boldsymbol{\lambda}_2 & \boldsymbol{\lambda}_3 & \boldsymbol{\lambda}_4 \end{bmatrix}. $$

Note that we make the force in y-direction zero because the second rows of $\boldsymbol{\lambda}_i,\ \forall i \in \{1,\cdots,4\}$ are zero.

Let us also introduce the thrust input vector $\boldsymbol{f}_{\text{r-}} = [f_1 - f_2\ f_3 - f_4]^\top$. Then, Eq. (9) can be simplified as

$$\tau_\chi = \begin{bmatrix} l_{fh} & l_{fh} \end{bmatrix} \boldsymbol{f}_{\text{r-}}. \tag{11}$$

Given a desired wrench $[{}^b f_{\text{rot}x}\ 0\ {}^b f_{\text{rot}z}\ {}^b\boldsymbol{\tau}_{\text{rot}}^\top]^\top$ and the torque τ_χ for the quadlink, the rotor thrust realizing them can be derived by the inverse transformation of Eqs. (10) and (11).

Remark 1: Because $\boldsymbol{f}_{\text{r+}}$ and $\boldsymbol{f}_{\text{r-}}$ have six elements with six rotors' thrusts, we can find one combination of rotors' thrusts for any pair of $\boldsymbol{f}_{\text{r+}}$ and $\boldsymbol{f}_{\text{r-}}$. Also, by definitions, any elements in $\boldsymbol{f}_{\text{r+}}$ and $\boldsymbol{f}_{\text{r-}}$ do not depend on other elements.

D. Aerodynamic Force

As the velocity of the vehicle increases, aerodynamic forces serve as an important factor. Suppose that the point of application of the aerodynamic force is the same as the vehicle's center of mass. Then, the aerodynamic force and torque in Σ_s are defined as

$${}^s\boldsymbol{f}_{\text{aero}} = \begin{bmatrix} -D & 0 & -L \end{bmatrix}^\top, \tag{12}$$

$${}^s\boldsymbol{\tau}_{\text{aero}} = \boldsymbol{0}, \tag{13}$$

with

$$D = \frac{1}{2}\rho {}^s v_x^2 \mathcal{S}\mathcal{C}_D, \tag{14}$$

$$L = \frac{1}{2}\rho {}^s v_x^2 \mathcal{S}\mathcal{C}_L, \tag{15}$$

that represent the drag and lift forces, respectively. Note that ρ represents air density, $\mathcal{S}$ is the wing area, and $\mathcal{C}_D$ and $\mathcal{C}_L$ are coefficients dependent on the angle of attack α. To determine $\mathcal{C}_D$ and $\mathcal{C}_L$, we approximate the results obtained from the work [20] using polynomial expressions.

III. REALIZABILITY OF THE CRUISE FLIGHT

A. Realizability Analysis

In this subsection, we analyze the feasibility of the cruise flight of the proposed VTOL UAV. We first define the cruise flight and clarify the conditions necessary for achieving it. Because the derived conditions provide appropriate values for the angle of attack and quadlink, α and χ, the acquired conditions will be utilized to plan α and χ during the flight in the next subsection.

Let us define the cruise flight considered in this paper.

Definition 1 (Cruise flight): Given a cruise speed ${}^s v_x > 0$, the UAV is regarded in the cruise flight if the following conditions are satisfied.

$${}^w\dot{\boldsymbol{x}} = [{}^s v_x\ 0\ 0]^\top,\ {}^b\dot{\boldsymbol{v}} = \boldsymbol{0},\ \dot{\boldsymbol{\eta}} = \boldsymbol{0},\ {}^b\dot{\boldsymbol{\omega}} = \boldsymbol{0}.$$

Note that the above definition implies that the UAV in the cruise phase flies at a constant altitude because its velocity is directed horizontally. In this setting, the x-y plane of the inertial frame Σ_w is parallel to the x-y plane of the stability frame Σ_s, resulting in a complete alignment between the angle of attack α and the pitch angle θ. Then, the equilibrium point in the cruise flight phase can be expressed as

$${}^b\boldsymbol{v} = \begin{bmatrix} {}^s v_x \cos\alpha & 0 & {}^s v_x \sin\alpha \end{bmatrix}^\top, \tag{16a}$$

$$\boldsymbol{\eta} = \begin{bmatrix} 0 & \alpha & 0 \end{bmatrix}^\top, \tag{16b}$$

$$\boldsymbol{\omega} = \begin{bmatrix} 0 & 0 & 0 \end{bmatrix}^\top. \tag{16c}$$

Let us denote the capability of the cruise flight, in the sense of Definition 1, as *cruisability* hereafter. Then, the cruisability of the proposed UAV can be analyzed by the following Lemma.

Lemma 1 (Cruisability check): The proposed UAV achieves a cruise flight if and only if the following two conditions are satisfied.

1) There exists input vector $\boldsymbol{f}_{r+}$ satisfying

$$\boldsymbol{M}\boldsymbol{f}_{r+} = \begin{bmatrix} -\boldsymbol{R}_y(\alpha)^\top ({}^s\boldsymbol{f}_{\text{aero}} + m\boldsymbol{g}) \\ \boldsymbol{O}_{3\times 1} \end{bmatrix}. \tag{17}$$

2) The control effectiveness matrix $\boldsymbol{M}$ satisfies

$$\text{rank}(\boldsymbol{M}) = 4.$$

The first condition in Lemma 1 indicates the existence of the equilibrium points, namely the existence of the thrust inputs that cancel out the combined force of gravity and the aerodynamic force, as in Fig. 4. The second condition assures the local controllability around the equilibrium point. Please refer to the authors' antecessors' work [18], which considers the hovering capability of the multi-rotor UAV with upward-oriented rotors, for details of the connection between the local controllability and the second condition.

For a given cruising speed, the above requirements provide us with the appropriate values of the angle of attack α and quadlink χ of the proposed UAV, as detailed in the next theorem.

Theorem 1: The proposed UAV realizes a cruise flight when the following conditions are satisfied.

1) ${}^s v_x$, α, and χ satisfy

$$\begin{aligned}(mg - L)\left(S_{\alpha+\chi} + \frac{l_f}{l_b} C_\chi S_\alpha\right) \\ + D\left(C_{\alpha+\chi} + \frac{l_f}{l_b} C_\chi C_\alpha\right) = 0.\end{aligned} \tag{18}$$

2) $\chi \neq \tan^{-1}(\kappa / l_{fw})$.

Note that Eq. (18) includes ${}^s v_x$ as a variable because D and L are the functions of ${}^s v_x$.

Proof: Each of the above two conditions corresponds with items 1 and 2 in Lemma 1. In the following, we derive each condition in order.

First, let us transform the condition (17) defined in the inertial frame into the stability frame as

$$\begin{bmatrix} \boldsymbol{R}_y(\alpha) & \boldsymbol{O}_3 \\ \boldsymbol{O}_3 & \boldsymbol{I}_3 \end{bmatrix} \boldsymbol{M}\boldsymbol{f}_{r+} + \begin{bmatrix} {}^s\boldsymbol{f}_{\text{aero}} + m\boldsymbol{g} \\ \boldsymbol{O}_{3\times 1} \end{bmatrix} = \boldsymbol{0}. \tag{19}$$

By substituting the equilibrium point (16) and allocating the same magnitude of thrust input symmetrically with respect

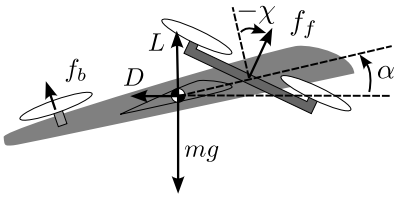

Fig. 4: The relationship of the forces at the equilibrium point.

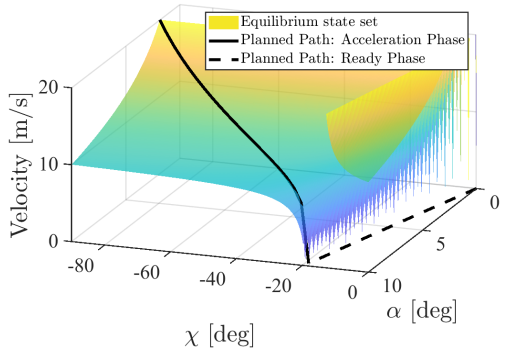

Fig. 5: The curve satisfying cruisability conditions.

to the x-axis of the body frame, namely $f_1 = f_3,\ f_2 = f_4,\ f_5 = f_6$, we obtain

$$\begin{bmatrix} -D - f_f \sin(\alpha+\chi) - f_b \sin(\alpha) \\ 0 \\ mg - L - f_f \cos(\alpha+\chi) - f_b \cos(\alpha) \\ 0 \\ f_f l_f \cos(\chi) - f_b l_b \cos(\chi) = 0 \\ 0 \end{bmatrix} = \begin{bmatrix} 0 \\ 0 \\ 0 \\ 0 \\ 0 \\ 0 \end{bmatrix}, \quad (20)$$

where $f_f = \sum_{i=1}^{4} f_i$ and $f_b = \sum_{i=5}^{6} f_i$. Note that Eq. (20) represents the condition where the force in the x and z direction and the torque around the y-axis are zero, as shown in Fig. 4. From (20), we can obtain the condition (18) in the first item.

Next, let us derive the condition for satisfying item 2 in Lemma 1. By splitting Eq. (10) as

$$\boldsymbol{M} = \left[\begin{array}{cc|cc} -S_\chi & -S_\chi & 0 & 0 \\ 0 & 0 & 0 & 0 \\ \hline -C_\chi & -C_\chi & -1 & -1 \\ -l_{fw}C_\chi - \kappa S_\chi & l_{fw}C_\chi + \kappa S_\chi & -l_{bw} & l_{bw} \\ \hline l_f C_\chi & l_f C_\chi & -l_b & -l_b \\ l_{fw}S_\chi - \kappa C_\chi & -l_{fw}S_\chi + \kappa C_\chi & \kappa & -\kappa \end{array}\right] = \left[\begin{array}{c|c} \boldsymbol{M}_{11} & \boldsymbol{M}_{12} \\ \hline \boldsymbol{M}_{21} & \boldsymbol{M}_{22} \\ \hline \boldsymbol{M}_{31} & \boldsymbol{M}_{32} \end{array}\right], \quad (21)$$

the following condition holds.

$$\mathrm{rank}(\boldsymbol{M}) = \mathrm{rank}(\boldsymbol{M}_{22}) + \mathrm{rank}\left(\begin{bmatrix} \boldsymbol{M}_{11} \\ \boldsymbol{M}_{31} \end{bmatrix}\right). \quad (22)$$

Note that $\mathrm{rank}(\boldsymbol{M}_{22}) = 2$ from the definition. In addition, $\mathrm{rank}([\boldsymbol{M}_{11}^\top \boldsymbol{M}_{31}^\top]^\top) = 2$ holds when $\chi \neq \tan^{-1}(\kappa/l_{fw})$ is satisfied, resulting in $\mathrm{rank}(\boldsymbol{M}) = 4$. This completes the proof. ■

Figure 5 illustrates the curve satisfying both conditions in Theorem 1 in a space with the x, y, and z axes representing χ, α, and the cruising speed ${}^s v_x$. On the curve, the equilibrium input exists, and from Theorem 1, the system can be cruisable.

B. Planning of α and χ

During the transition phase, the UAV is required to change its angle of attack α and tilt angle of quadlink χ to accelerate its body. However, α and χ have to take close enough value to the condition derived in Theorem 1 to make the UAV controllable. To achieve this goal, we utilize the curve in Fig. 5, derived from Theorem 1, for planning α and χ. In Fig. 5, the black line and dashed line represent the planned path for acceleration and ready phase, respectively. For both transitions, we design paths so that α and χ change linearly.

As mentioned at the end of Section II-A and Fig. 3, during the ready phase, the UAV tilts its quadlink forward to prepare for the acceleration phase. At the same time, the angle of attack has to increase to keep the cruising speed ${}^s v_x = 0$ during the ready phase and acquire enough aerodynamic force to maintain its altitude even with a small cruising speed at the beginning of the subsequent acceleration phase. Once the UAV moves to the acceleration phase, the UAV increases its cruising speed by tilting quadlink forward more. As the cruising speed becomes large, a small angle of attack is enough to generate necessary lifting forces.

Note that the point $(\chi, \alpha, {}^s v_x)$ on the curve in Fig. 5 signifies the equilibrium point at which the thrust input achieving the cruise flight exists with the designated χ and α. Nevertheless, in the acceleration phase, the UAV is required to increase its cruise speed rather than stay at the equilibrium point. To achieve this goal, we have to shift the value of χ or α from the equilibrium point. In this paper, we opt for changing χ rather than α because the deviation in the angle of attack causes the change of aerodynamic force, which necessitates a more complicated analysis as Eqs. (14) and (15) are nonlinear. The controller in the following section is designed to control χ to accelerate the vehicle rather than changing α from its value at the equilibrium point.

IV. CONTROLLER

In this section, we present a comprehensive controller that encompasses the control of the UAV's body and the tilt angle of the quadlink. The overview of the designed controller is shown in Fig. 6, which is composed of four main components: position controller, attitude controller, control allocation, and tilt angle controller. Among them, we use two types of position controllers; one is for the hovering phase, and the other is for other phases.

In all phases of flight, the controller receives time-series data of the reference forward velocity ${}^s v_x$, seen in the stability frame, and the angle of attack α. The UAV is then controlled by adjusting rotor thrusts and dynamically changing the tilt angle of the quadlink, χ. Note that, as mentioned in Section III-A, the angle of attack α and the pitch angle θ take the same value when the vehicle moves

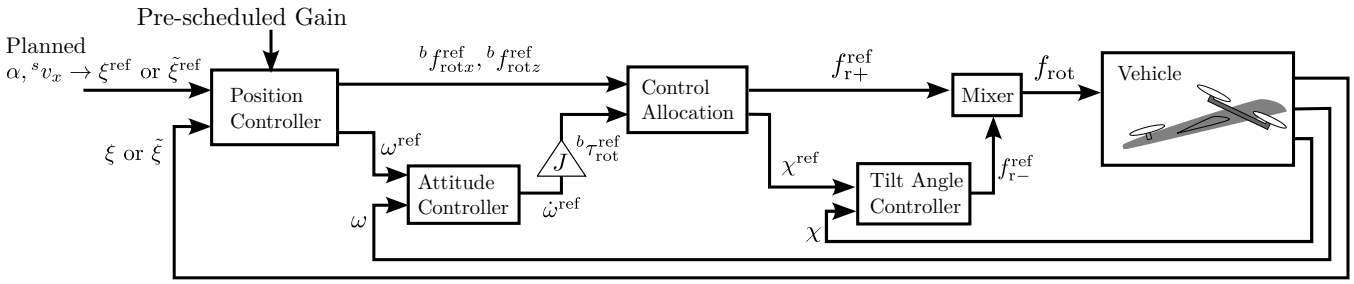

Fig. 6: The overall architecture of the proposed controller.

to the x-direction of the inertial frame, as in the case of this paper. Hence, the planned α is utilized as the reference of the pitch angle θ, and we often use α and θ interchangeably hereafter. Also, in this section, we denote the reference value obtained from pre-planned values or a controller as $*^{\text{ref}}$.

A. Position Controller for Hovering Phase

The position controller for the hovering phase utilizes the LQR-optimal control. The state vector is represented as $\boldsymbol{\xi} = [{}^w\boldsymbol{x}^\top \ {}^b\boldsymbol{v}^\top \ \boldsymbol{\eta}^\top]^\top$, and the input vector as $\boldsymbol{u} = [{}^b f^{\text{ref}}_{\text{rot}z} \ {}^b\boldsymbol{\omega}^{\text{ref}\top}]^\top$. The reference vector $\boldsymbol{\xi}^{\text{ref}}$ is denoted as

$$\boldsymbol{\xi}^{\text{ref}} = \begin{bmatrix} 0 & 0 & z^{\text{ref}} & 0 & 0 & 0 & 0 & 0 & 0 \end{bmatrix}^\top, \tag{23}$$

where $z^{\text{ref}} \in \mathbb{R}$ is a reference altitude. By employing $\boldsymbol{\xi}$ and transforming Eq. (3), the nonlinear state space equation can be obtained as

$$\dot{\boldsymbol{\xi}} = h(\boldsymbol{\xi}, \boldsymbol{u}). \tag{24}$$

Note that Eq. (24) does not include the aerodynamic forces, as it can be neglected in the hovering phase. The nonlinear system (24) can be linearized using a first-order Taylor approximation around the reference equilibrium state (23) as

$$\dot{\boldsymbol{\xi}} = \frac{\partial h}{\partial \boldsymbol{\xi}}(\boldsymbol{\xi}=\boldsymbol{\xi}^{\text{ref}}, \boldsymbol{u}=\boldsymbol{0})\boldsymbol{\xi} + \frac{\partial h}{\partial \boldsymbol{u}}(\boldsymbol{\xi}=\boldsymbol{\xi}^{\text{ref}}, \boldsymbol{u}=\boldsymbol{0})\boldsymbol{u}. \tag{25}$$

We then apply LQR-optimal control, with the weight matrices $\boldsymbol{Q}_{\text{hover}}$ and $\boldsymbol{R}_{\text{hover}}$ for states and inputs, to determine the feedback gain.

B. Position Controller for the Other Phases

The position controller for other flight phases follows a similar scheme to the one in the hovering phase. Still, some modifications to the position controller are necessitated in order to mitigate unfavorable interference between the pitch angle θ, which can be regarded as the angle of attack α as mentioned at the beginning of this section, and the other state variables. More specifically, as shown in (3a) and (3c), the pitch angle θ influences the position and velocity of the UAV. In the control of a traditional multi-rotor UAV with untiltable rotors and no wings, this relationship can be utilized in a way that the UAV accelerates by tilting its body forward. However, in our newly designed UAV, this behavior should be avoided as tilting the body itself forward means heading the nose of the UAV downward, where the UAV cannot generate the lifting force by the aerodynamic force and could fall. For this goal, we propose a control method utilizing exact linearization of the pitch angle θ through coordinate transformation and nonlinear feedback. This approach allows us to control the pitch angle θ independently from other variables, ensuring θ follows a pre-planned value. As a result, the proposed scheme favors utilizing χ rather than θ to accelerate the UAV's body. Note that remaining angles such as roll and yaw are necessary for controlling the position and velocity in the y-direction. This is because the vehicle does not generate the force in the y-direction. Therefore, the system is exactly linearized for the pitch angle only.

Let the new velocity vector be $\tilde{\boldsymbol{v}} = \boldsymbol{R}_y(\theta)^b\boldsymbol{v}$, the new force vector be $\tilde{\boldsymbol{f}}_{\text{rot}} = \boldsymbol{R}_y(\theta)^b\boldsymbol{f}_{\text{rot}}$, and the new state and the input vector be

$$\tilde{\boldsymbol{\xi}} = \begin{bmatrix} {}^w\boldsymbol{x}^\top & \tilde{\boldsymbol{v}}^\top & \boldsymbol{\eta}^\top \end{bmatrix}^\top, \tag{26}$$

$$\tilde{\boldsymbol{u}} = \begin{bmatrix} \tilde{f}^{\text{ref}}_{\text{rot}x} & \tilde{f}^{\text{ref}}_{\text{rot}z} & \dot{\boldsymbol{\eta}}^\top \end{bmatrix}^\top. \tag{27}$$

From the previously planned value ${}^s v_x^{\text{ref}}$ and α^{ref} in Section III-B, the reference vector $\tilde{\boldsymbol{\xi}}^{\text{ref}}$ is determined as

$$\tilde{\boldsymbol{\xi}}^{\text{ref}} = \begin{bmatrix} * & 0 & z^{\text{ref}} & {}^s v_x^{\text{ref}} C_{\alpha^{\text{ref}}} & 0 & {}^s v_x^{\text{ref}} S_{\alpha^{\text{ref}}} & 0 & \alpha^{\text{ref}} & 0 \end{bmatrix}^\top. \tag{28}$$

Note that $*$ at the x-element signifies we do not control x. Instead, we control the cruise speed ${}^s v_x$. Then, the system is exactly linearized in terms of the pitch angle θ as

$$\begin{aligned} \dot{\tilde{\boldsymbol{\xi}}} &= \tilde{h}(\tilde{\boldsymbol{\xi}}, \ \tilde{\boldsymbol{u}}) \\ &= \begin{bmatrix} \boldsymbol{R}_z(\psi)\boldsymbol{R}_x(\phi)\tilde{\boldsymbol{v}} \\ \frac{{}^s\boldsymbol{f}_{\text{aero}}}{m} + \boldsymbol{R}_x(\phi)^\top \boldsymbol{R}_z(\psi)^\top \boldsymbol{g} \\ \boldsymbol{O}_3 \end{bmatrix} + \begin{bmatrix} \boldsymbol{O}_{3\times 2} & \boldsymbol{O}_3 \\ \frac{1}{m} \quad 0 & \\ 0 \quad\ 0 & \boldsymbol{O}_3 \\ 0 \quad \frac{1}{m} & \\ \boldsymbol{O}_{3\times 2} & \boldsymbol{I}_3 \end{bmatrix} \tilde{\boldsymbol{u}}. \end{aligned} \tag{29}$$

Notice that the first six rows in (29) do not include $\tilde{\theta}$, and the right bottom block of the matrix multiplied to $\tilde{\boldsymbol{u}}$ is the identity matrix; hence $\tilde{\theta}$ only depends on the input $\tilde{\boldsymbol{u}}$ and can independently control it. Finally, the control input $\tilde{\boldsymbol{u}}$ for the above model can be transformed in the form of $[f^{\text{ref}}_{\text{rot}x} \ f^{\text{ref}}_{\text{rot}z} \ {}^b\boldsymbol{\omega}^{\text{ref}\top}]^\top$, which is the same form as in the hovering controller.

Similar to the hovering phase, the nonlinear system (29) can be linearized around the equilibrium state (28) as

$$\dot{\tilde{\boldsymbol{\xi}}} = \frac{\partial \tilde{h}}{\partial \tilde{\boldsymbol{\xi}}}(\tilde{\boldsymbol{\xi}}=\tilde{\boldsymbol{\xi}}^{\text{ref}}, \tilde{\boldsymbol{u}}=\boldsymbol{0})\tilde{\boldsymbol{\xi}} + \frac{\partial \tilde{h}}{\partial \tilde{\boldsymbol{u}}}(\tilde{\boldsymbol{\xi}}=\tilde{\boldsymbol{\xi}}^{\text{ref}}, \tilde{\boldsymbol{u}}=\boldsymbol{0})\tilde{\boldsymbol{u}}. \tag{30}$$

We apply LQR-optimal control, with the weight matrices $\boldsymbol{Q}_{\text{cruise}}$ and $\boldsymbol{R}_{\text{cruise}}$ for states and inputs, to determine the feedback gain. The feedback gain of each timestep is calculated previously offline.

C. Attitude Controller

The attitude controller renders a reference angular acceleration ${}^b\dot{\boldsymbol{\omega}}^{\text{ref}}$ for a fuselage to make ${}^b\boldsymbol{\omega}$ follow a reference ${}^b\boldsymbol{\omega}^{\text{ref}}$. We employ a PID controller with P-, I-, and D-gains, K_P^A, K_I^A, and K_D^A, respectively.

D. Control Allocation

The control allocation derives a reference χ^{ref} and $\boldsymbol{f}_{\text{r+}}^{\text{ref}}$ that achieves ${}^b f_{\text{rot}x}^{\text{ref}}$, ${}^b f_{\text{rot}z}^{\text{ref}}$, ${}^b\boldsymbol{\tau}_{\text{rot}}^{\text{ref}} = \boldsymbol{J}{}^b\dot{\boldsymbol{\omega}}^{\text{ref}}$ calculated by the position and attitude controllers. For this goal, the position controller finds χ and $\boldsymbol{f}_{\text{r+}}$ satisfying Eq. (10), which is reproduced as

$$\begin{bmatrix} {}^b f_{\text{rot}x}^{\text{ref}} \\ 0 \\ {}^b f_{\text{rot}z}^{\text{ref}} \\ {}^b\boldsymbol{\tau}_{\text{rot}}^{\text{ref}} \end{bmatrix} = \boldsymbol{M}(\chi^{\text{ref}})\boldsymbol{f}_{\text{r+}}^{\text{ref}}. \tag{31}$$

Note that, in the hovering phase, we substitute $\chi^{\text{ref}} = 0$ and $f_{\text{rot}x}^{\text{ref}} = 0$ into (31) before obtaining $\boldsymbol{f}_{\text{r+}}^{\text{ref}}$.

Let us emphasize that the reference thrust $\boldsymbol{f}_{\text{r+}}^{\text{ref}}$ only designates the thrust of two rotors at the tail and the summations of two rotors located on the same side of the quadlink. In other words, $\boldsymbol{f}_{\text{r+}}^{\text{ref}}$ does not specify the thrust of each rotor mounted on the quadlink, namely $f_i,\ i = \{1 \cdots 4\}$. These values are determined by mixing $\boldsymbol{f}_{\text{r+}}^{\text{ref}}$ and $\boldsymbol{f}_{\text{r-}}^{\text{ref}}$, as explained in the next subsection.

E. Tilt Angle Controller

The tilt angle controller calculates $\boldsymbol{f}_{\text{r-}} = [f_1 - f_2\ f_3 - f_4]^\top$, which makes χ follows a reference value χ^{ref}. Since $\boldsymbol{f}_{\text{r-}}^{\text{ref}}$ is the difference of thrust between the front and rear rotors in the quadlink, combining $\boldsymbol{f}_{\text{r+}}$ and $\boldsymbol{f}_{\text{r-}}$ via a mixer determines each rotor's thrust in the quadlink, as mentioned in Remark 1. We employ a PID controller to obtain the reference torque input τ_χ^{ref}, which is utilized to yield $\boldsymbol{f}_{\text{r-}}^{\text{ref}}$ as

$$\boldsymbol{f}_{\text{r-}}^{\text{ref}} = \begin{bmatrix} l_{fh} & l_{fh} \end{bmatrix}^\dagger \tau_\chi^{\text{ref}}, \tag{32}$$

where $\dagger$ denotes the Moore-Penrose inverse. P-, I-, and D-gains are K_P^χ, K_I^χ, and K_D^χ, respectively.

V. Simulation

This section presents simulation study, where we demonstrate the proposed control strategy successfully achieves a transition from hovering to cruise flight mode. The simulation also verifies that the proposed method converges to the desired cruising speed, the angle of attack, and the tilt angle of the quadlink specified by Theorem 1 in the cruise flight mode. The parameters of the vehicle are set as $m = 0.5$ kg, $\boldsymbol{J} = \text{diag}(0.03, 0.05, 0.05)$ kgm^2, and $l_f = l_{fw} = l_{fh} = l_b = l_{bw} = 0.1$ m, with setting the inertial moment of the quadlink as 0.01 kgm^2. Also, the control gains are $\boldsymbol{Q}_{\text{hover}} = \text{diag}(1, 1, 10, 1, 1, 1, 1, 1, 1)$, $\boldsymbol{R}_{\text{hover}} = \text{diag}(1, 2, 2, 1) \times 10^2$, $\boldsymbol{Q}_{\text{cruise}} = \text{diag}(1, 1, 10^2, 10^4, 1, 10^4, 1, 10^3, 1)$, $\boldsymbol{R}_{\text{cruise}} = \text{diag}(31, 31, 2, 2, 2) \times 10^2$, $[K_P^A,\ K_I^A,\ K_D^A] = [100, 1000, 0.3]$, and $[K_P^\chi,\ K_I^\chi,\ K_D^\chi] = [5, 1, 4]$.

By denoting the simulation time as t, the performed simulation can be divided into the following three phases:

- From the initial z-position $z = 0$, the UAV moves to the desired z-position $z = -5$ (altitude of 5 m) and keep hovering until $t = 20$ s,
- the UAV is in the ready phase from $t = 20$ s to $t = 30$ s, where α and χ converge the desired value at $t = 25$ s and hover until $t = 30$ s with fixing α and χ, and
- the UAV is in the acceleration phase from $t = 30$ s to $t = 50$ s, and
- the UAV is in the cruise phase from $t = 50$ s to $t = 80$ s, with ${}^w v_x = 20$ m/s.

Note that, in all phases, the UAV's reference y-position is $y = 0$. The above reference trajectories of ${}^w v_x$, ${}^w y$, and ${}^w z$ are depicted in black dashed lines in Figs. 8(a) and 8(e).

The evolution of all states of the UAV during simulation is shown in Fig. 8. All the values, except for the body angular velocity in Fig. 8(f), are seen in the inertial frame. Fig. 8(a) depicts the cruising speed, and Fig. 8(b) shows the roll, pitch, and yaw angle. Also, the evolution of χ is illustrated in Fig. 8(c).

Let us investigate the evolution of ${}^s v_x$, θ, and χ, shown in Figs. 8(a), 8(b), and 8(c). The black dashed line in Fig. 8(b) and the orange dashed line in Fig. 8(c) correspond with the planned value in Fig. 5, calculated from Theorem 1. Let us emphasize that, as mentioned in Sections III and IV, this planned value corresponds with the equilibrium points, and hence, during the acceleration phase, the tilt angle of the quadlink has to deviate from the path in order to accelerate or decelerate, as detailed soon. First, in the hovering phase, although a deviation of θ can be confirmed before the UAV converges to $z = -5$ m, its effect on the cruising speed ${}^s v_x$ and y, z positions is small and can be negligible. Second, in the ready phase, ${}^s v_x$, θ, and χ follow the planned values, and the UAV achieves static hovering, i.e., its position does not change, as shown in Fig. 8(e). In the acceleration phase, as mentioned earlier, the proposed control design tilts the quadlink forward than the path generated from the equilibrium conditions to accelerate, as in Fig. 8(c). Notably, the cruise speed ${}^s v_x$ and the pitch angle θ, corresponding to the angle of attack α, do not deviate from the planned path, hence restraining the change of the aerodynamic force from the planned one. This strategy alleviates the complicated effect of the aerodynamic force. During this acceleration phase, z-position shows slight changes from the reference. This deviation can be regarded as a price of increasing the cruise speed because tilting quadlink forward leads to a decrease of the force canceling the gravity. Nevertheless, as the cruising speed increases, this deviation is eliminated. Lastly, in the cruise phase, all the state of the UAV converges the planned one, namely the equilibrium point, and achieving the cruise flight with the desired cruising speed. The above results demonstrate the proposed control

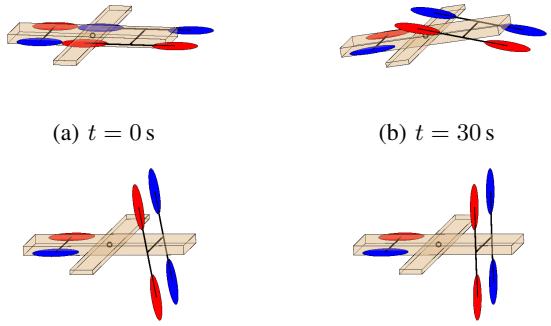

(a) $t = 0\,\mathrm{s}$ (b) $t = 30\,\mathrm{s}$

(c) $t = 50\,\mathrm{s}$ (d) $t = 80\,\mathrm{s}$

Fig. 7: Snapshots illustrating attitude and χ of the UAV, where the UAV moves from left to right.

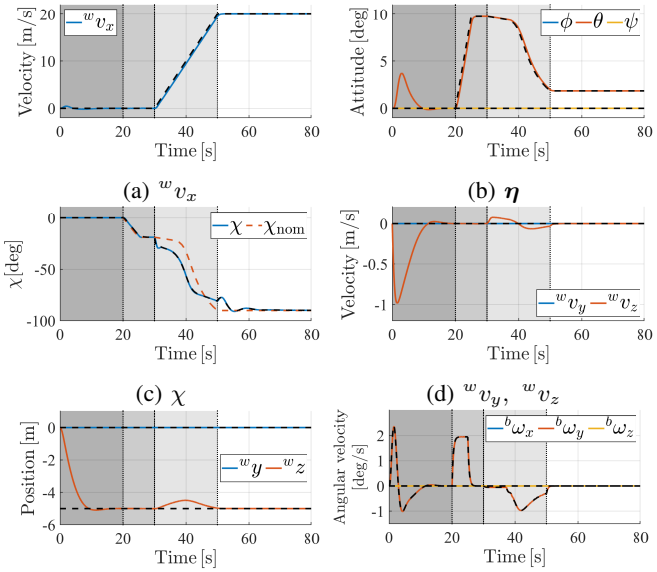

(a) ${}^{w}v_x$ (b) $\boldsymbol{\eta}$

(c) χ (d) ${}^{w}v_y$, ${}^{w}v_z$

(e) ${}^{w}y$, ${}^{w}z$ (f) ${}^{b}\boldsymbol{\omega}$

Fig. 8: Simulation results, where four flight phases are highlighted in the different background colors.

strategy successfully achieve the transitions of flight mode, while achieving the cruise flight with the desired cruising speed.

VI. CONCLUSION

This paper presented a novel VTOL UAV having six rotors, four of which are mounted to a tiltable link attached to the fuselage via a passive joint. We first presented the flight modes for the designed UAV while describing the overall strategy of manipulating the angle of attack and the tilt angle of the quadlink. We derived the dynamical model of the UAV and analyzed its controllability. The derived condition for the UAV's controllability is utilized for planning the angle of attack and the tilt angle of the quadlink. We then designed the controller that leverages the tiltable quadlink to accelerate the UAV while the deviations in the angle of attack from the equilibrium value are suppressed to avoid the changes of the aerodynamic force. The validity of the designed UAV and the proposed controller are demonstrated in simulation studies.

REFERENCES

[1] M. Mammarella, C. Donati, T. Shimizu, M. Suenaga, L. Comba, A. Biglia, K. Uto, T. Hatanaka, P. Gay, and F. Dabbene, "3D map reconstruction of an orchard using an angle-aware covering control strategy," *IFAC-PapersOnLine*, vol. 55, no. 32, pp. 271–276, 2022.

[2] W. Eikyu, K. Sekiguchi, and K. Nonaka, "Nonlinear control for the extended model of the load-suspended UAV based on the experiments," *IFAC-PapersOnLine*, vol. 54, no. 14, pp. 90–95, 2021.

[3] M. Erdelj, E. Natalizio, K. R. Chowdhury, and I. F. Akyildiz, "Help from the sky: Leveraging UAVs for disaster management," *IEEE Pervasive Computing*, vol. 16, no. 1, pp. 24–32, 2017.

[4] M. A. Boon, A. P. Drijfhout, and S. Tesfamichael, "Comparison of a fixed-wing and multi-rotor UAV for environmental mapping applications: A case study," *Int. Arch. Photogrammetry, Remote Sensing and Spatial Information Sci.*, vol. XLII-2/W6, pp. 47–54, 2017.

[5] A. S. Saeed, A. B. Younes, C. Cai, and G. Cai, "A survey of hybrid unmanned aerial vehicles," *Prog. Aerospace Sci.*, vol. 98, pp. 91–105, 2018.

[6] S. Kohno and K. Uchiyama, "Design of robust controller of fixed-wing UAV for transition flight," in *Int. Conf. on Unmanned Aircraft Syst.*, 2014, pp. 1111–1116.

[7] B. Li, J. Sun, W. Zhou, C.-Y. Wen, K. H. Low, and C.-K. Chen, "Transition optimization for a VTOL tail-sitter UAV," *IEEE/ASME Trans. Mechatronics*, vol. 25, no. 5, pp. 2534–2545, 2020.

[8] E. Tal, G. Ryou, and S. Karaman, "Aerobatic trajectory generation for a VTOL fixed-wing aircraft using differential flatness," *IEEE Trans. Robot.*, pp. 1–15, 2023.

[9] C. Kikumoto, T. Urakubo, K. Sabe, and Y. Hazama, "Back-transition control with large deceleration for a dual propulsion VTOL UAV based on its maneuverability," *IEEE Robot. Autom. Lett.*, vol. 7, no. 4, pp. 11 697–11 704, 2022.

[10] Z. Liu, Y. He, L. Yang, and J. Han, "Control techniques of tilt rotor unmanned aerial vehicle systems: A review," *Chinese J. Aeronautics*, vol. 30, no. 1, pp. 135–148, 2017.

[11] R. G. Hernández-García and H. Rodríguez-Cortés, "Transition flight control of a cyclic tiltrotor UAV based on the gain-scheduling strategy," in *Int. Conf. Unmanned Aircraft Syst.*, 2015, pp. 951–956.

[12] ——, "A total energy control system design for the transition phase of a tiltrotor aerial vehicle," *IFAC Proc. Vol.*, vol. 46, no. 30, pp. 52–57, 2013.

[13] X. Fang, Q. Lin, Y. Wang, and L. Zheng, "Control strategy design for the transitional mode of tiltrotor UAV," in *IEEE Int. Conf. Industrial Informatics*, 2012, pp. 248–253.

[14] D. Rohr, M. Studiger, T. Stastny, N. R. J. Lawrance, and R. Siegwart, "Nonlinear model predictive velocity control of a VTOL tiltwing UAV," *IEEE Robot. Autom. Lett.*, vol. 6, no. 3, pp. 5776–5783, 2021.

[15] M. Allenspach and G. J. Ducard, "Model predictive control of a convertible tiltrotor unmanned aerial vehicle," in *Mediterranean Conf. Control and Autom.*, 2020, pp. 715–720.

[16] M. Mousaei, J. Geng, A. Keipour, D. Bai, and S. Scherer, "Design, modeling and control for a tilt-rotor VTOL UAV in the presence of actuator failure," in *IEEE/RSJ Int. Conf. Intelligent Robots and Syst.*, 2022, pp. 4310–4317.

[17] R. Chiappinelli, M. Cohen, M. Doff-Sotta, M. Nahon, J. R. Forbes, and J. Apkarian, "Modeling and control of a passively-coupled tilt-rotor vertical takeoff and landing aircraft," in *2019 International Conference on Robotics and Automation*, 2019, pp. 4141–4147.

[18] S. Mochida, R. Matsuda, T. Ibuki, and M. Sampei, "A geometric method of hoverability analysis for multirotor UAVs with upward-oriented rotors," *IEEE Trans. Robot.*, vol. 37, no. 5, pp. 1765–1779, 2021.

[19] T. Hatanaka, N. Chopra, M. Fujita, and M. W. Spong, *Passivity-Based Control and Estimation in Networked Robot.* Springer, 2015.

[20] U. Ozdemir, Y. O. Aktas, A. Vuruskan, Y. Dereli, A. F. Tarhan, K. Demirbag, A. Erdem, G. D. Kalaycioglu, I. Ozkol, and G. Inalhan, "Design of a commercial hybrid VTOL UAV system," *J. Intelligent & Robot. Syst.*, vol. 74, no. 1, pp. 371–393, Apr. 2014.